Light-induced force and torque on an atom outside a nanofiber

Fam Le Kien,[1,*] V. I. Balykin,[1,2] and K. Hakuta[1]
[1]*Department of Applied Physics and Chemistry, University of Electro-Communications, Chofu, Tokyo 182-8585, Japan*
[2]*Institute of Spectroscopy, Troitsk, Moscow Region 142092, Russia*
(Received 29 April 2006; published 21 September 2006)

We study the action of the force and torque induced by a guided light field on a cesium atom outside a nanofiber. We demonstrate that the evanescent light field in a circular fundamental guided mode can force the atom to rotate around the nanofiber for a macroscopic time. We find that, due to the action of the torque, the angular momentum of the atom increases with time.

DOI: 10.1103/PhysRevA.74.033412 PACS number(s): 42.50.Vk, 32.80.Lg, 32.80.Pj, 32.80.−t

I. INTRODUCTION

The tightly confining traps of cold atoms allow one to envisage a broad spectrum of applications ranging from highly sensitive sensors to quantum information technology [1,2]. With the use of microstructured surfaces (atom chips), it becomes possible to confine and manipulate cold atoms on the micrometer-length scale [1,2]. Microtraps used in the previous experiments are magnetic traps produced by current-carrying wires or periodically magnetized surfaces. Recently, the limitations of the coherent manipulation of neutral atoms have been found in the traps based on current-carrying wires [3,4]. An alternative way for tightly confining of cold atoms is based on a *photon-carrying nanofiber* [5,6]. The method requires the use of a single (red-detuned) light beam [5] or two (red- and blue-detuned) light beams [6] launched into the fiber. In the single-color scheme [5], the trapping is achieved by the balance between the optical dipole force of a red-detuned light field and the centrifugal force on a spinning atom. In the two-color scheme [6], the trapping is achieved by the balance between the optical dipole forces of a red-detuned light field and a blue-detuned light field. The optical dipole forces used in the above schemes are produced by the gradient of the field intensity in the radial direction. Such forces are conservative. When the fields are far from resonance with the atom, the dissipative forces are negligible. With anticipation of preserving the coherence of the matter waves, a photon-carrying nanofiber could be a more quiet environment for cold atoms than a current-carrying microwire.

When the guided light field is not very far from resonance with the atom outside the nanofiber, the force of light on the atom is complicated. Because of the specifics of the nanofibers, the electric and magnetic field vectors of a guided mode have three different substantial components: axial, radial, and azimuthal [7]. Consequently, the Poynting vector for the field in a circular fundamental guided mode has two different substantial components, axial and azimuthal, which lead to axial and azimuthal pressure forces on the atom. These forces are substantial when the detuning of the field is not very large compared to the absorption linewidth of the atom. The axial force influences the translational motion of the atom along the fiber. The azimuthal force yields a torque that influences the rotational motion of the atom around the fiber.

In this paper, we study the action of the light-induced force and torque on a cesium atom outside a photon-carrying nanofiber. We demonstrate that the evanescent light field in a circular fundamental guided mode can force the atom to rotate around the nanofiber for a macroscopic time, with an increasing angular momentum.

The paper is organized as follows. In Sec. II, we describe the model. In Sec. III, we derive the basic equations for the internal state and center-of-mass motion of the atom. In Sec. IV, we present numerical results. Our conclusions are given in Sec. V.

II. MODEL

We consider a cesium atom interacting with light in a circular fundamental mode of a subwavelength-diameter single-mode fiber (nanofiber) (see Fig. 1). The thin fiber has a cylindrical silica core of radius a and refractive index n_1 and an infinite vacuum clad of refractive index $n_2=1$.

A. Evanescent light field outside the fiber

We first describe the guided light field. The frequency, free-space wave number, and free-space wavelength of the field are denoted by ω, $k=\omega/c$, and $\lambda=2\pi/k$, respectively. For certainty, we assume that the rotation direction of the field polarization around the fiber axis z is counterclockwise.

We represent the electric component of the field as $\mathbf{E}=(\boldsymbol{\mathcal{E}}e^{-i\omega t}+\boldsymbol{\mathcal{E}}^* e^{i\omega t})/2$. We introduce the notation $\mathcal{E}_{-1}=(\mathcal{E}_x-i\mathcal{E}_y)/\sqrt{2}$, $\mathcal{E}_0=\mathcal{E}_z$, and $\mathcal{E}_1=-(\mathcal{E}_x+i\mathcal{E}_y)/\sqrt{2}$ for the spherical tensor components of the field envelope vector $\boldsymbol{\mathcal{E}}$. Outside the fiber, in the cylindrical coordinates $\{r,\varphi,z\}$, the spherical tensor components of the field are given by [7,8]

$$\mathcal{E}_{-1}=\sqrt{2}\,i\mathcal{N}(1-s)K_0(qr)e^{i\beta z},$$

$$\mathcal{E}_0=\mathcal{N}\frac{2q}{\beta}K_1(qr)e^{i(\beta z+\varphi)},$$

$$\mathcal{E}_1=-\sqrt{2}i\mathcal{N}(1+s)K_2(qr)e^{i(\beta z+2\varphi)}. \quad (1)$$

Here, β is the axial propagation constant for the fiber fundamental mode, $q=(\beta^2-n_2^2k^2)^{1/2}$ characterizes the decay of the

*Also at Institute of Physics and Electronics, Vietnamese Academy of Science and Technology, Hanoi, Vietnam.

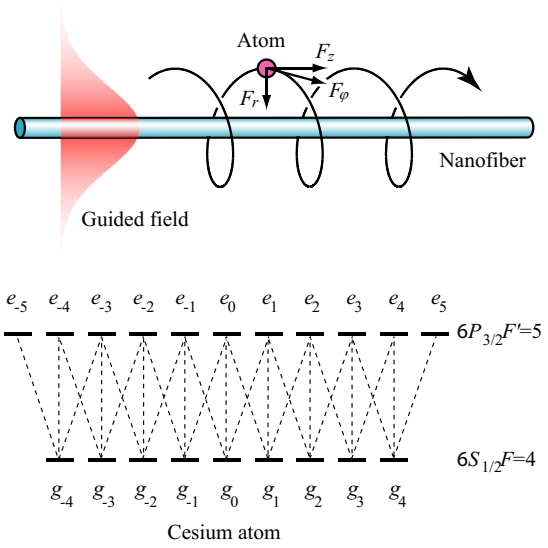

FIG. 1. (Color online) Upper part: Components of the light-induced force on an atom outside a nanofiber. Lower part: Schematic of the $6P_{3/2}F'=5$ and $6S_{1/2}F=4$ hyperfine-structure (hfs) levels of a cesium atom.

field outside the fiber, and s is defined as $s=(1/q^2a^2+1/h^2a^2)/[J_1'(ha)/haJ_1(ha)+K_1'(qa)/qaK_1(qa)]$, with $h=(n_1^2k^2-\beta^2)^{1/2}$ being a parameter for the field inside the fiber. The coefficient $\mathcal{N}$ characterizes the amplitude of the field. The notation J_n and K_n stand for the Bessel functions of the first kind and the modified Bessel functions of the second kind, respectively.

We note that, for conventional, weakly guiding fibers [7], the components $\mathcal{E}_1$ and $\mathcal{E}_0$ are negligible as compared to $\mathcal{E}_{-1}$. However, for subwavelength-diameter fibers, $\mathcal{E}_1$ and $\mathcal{E}_0$ are not negligible at all [9]. In the close vicinity of the surface of a thin fiber, the components $\mathcal{E}_{-1}$, $\mathcal{E}_0$, and $\mathcal{E}_1$ are comparable to each other. The effects of these components on the atom are of the same order. Therefore, we must include all the three components of the field in the calculations for the atomic state.

An important characteristic of the light propagation is the cycle-averaged Poynting vector $\mathbf{S}=(1/2)\mathrm{Re}(\boldsymbol{\mathcal{E}}\times\boldsymbol{\mathcal{H}}^*)$. Here, $\boldsymbol{\mathcal{H}}$ is the envelope vector of the magnetic component of the field. The parameter $P_z=\int_0^{2\pi}d\varphi\int_0^\infty S_z r dr$, which is the integral of the axial flow of energy S_z over the transverse plane of the fiber, is the propagation power of light. Since the mode considered is a guided mode, the radial component of the Poynting vector is vanishing, that is, $S_r=0$. The explicit expressions for the axial component S_z and the azimuthal component S_φ of the Poynting vector are given in Ref. [10]. In the case of conventional weakly guiding fibers [7], S_φ is small compared to S_z. However, in the case of nanofibers, S_φ is comparable to S_z (see Fig. 2). The component S_φ describes the energy flow that circulates around the fiber. The presence of this flow is a consequence of the fact that the longitudinal component of the field in the fundamental mode is not zero.

Outside the fiber, the linear and angular momentum densities of the electromagnetic field are given by $\mathbf{p}=\mathbf{S}/c^2$ and $\mathbf{j}\equiv[\mathbf{r}\times\mathbf{p}]=[\mathbf{r}\times\mathbf{S}]/c^2$, respectively [11]. The axial flow of energy S_z produces the axial linear momentum density $p_z=S_z/c^2$. The azimuthal flow of energy S_φ produces the azimuthal linear momentum density $p_\varphi=S_\varphi/c^2$. Note that S_φ also produces the angular momentum density $j_z=rS_\varphi/c^2$ with respect to the fiber axis [10].

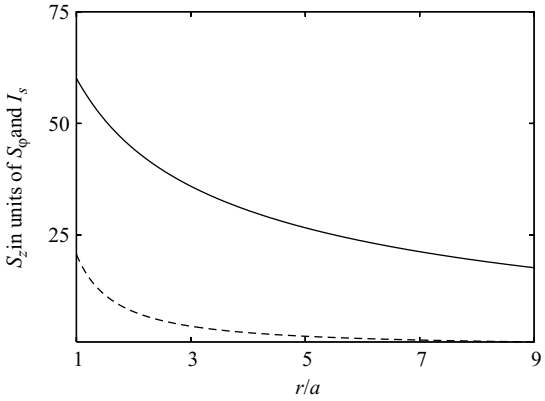

FIG. 2. Axial component S_z (solid line) and azimuthal component S_φ (dashed line) of the Poynting vector, normalized to the saturation intensity $I_s=1.1$ mW/cm^2. The fiber radius is $a=100$ nm, the refractive indices of the fiber and the vacuum clad are $n_1=1.45$ and $n_2=1$, respectively, the light wavelength is $\lambda=852$ nm, the light polarization is counterclockwise rotating, and the light propagation power is $P_z=10$ nW.

B. Atom–field interaction

We now examine the interaction of the cesium atom with the evanescent light field outside the fiber. We consider the hyperfine-structure (hfs) magnetic substates $|FM\rangle\equiv|LSJIFM\rangle$ and $|F'M'\rangle\equiv|L'SJ'IF'M'\rangle$ of a lower state $|LJ\rangle$ and an upper state $|L'J'\rangle$, respectively. Here L, S, J, I, F, and M are the quantum numbers for the orbital electronic angular momentum, electronic spin, total electronic angular momentum, nuclear spin, total atomic angular momentum, and magnetic momentum, respectively. The electronic and nuclear spins of atomic cesium are $S=1/2$ and $I=7/2$. We study the D_2 line, which occurs at the wavelength $\lambda_0=852$ nm and corresponds to the transition from the ground state $6S_{1/2}$ (with $L=0$ and $J=1/2$) to the excited state $6P_{3/2}$ (with $L'=1$ and $J'=3/2$). We assume that the cesium atom is initially prepared in the hfs level $F=4$ of the ground state $6S_{1/2}$ and that the field is tuned close to resonance with the hfs level $F'=5$ of the excited state $6P_{3/2}$ (see the lower part of Fig. 1). Among the hfs components of the D_2 line, the transition $6S_{1/2}F=4\leftrightarrow 6P_{3/2}F'=5$ has the strongest oscillator strength. Because of the selection rule $\Delta F=0,\pm1$, spontaneous emission from the excited hfs level $6P_{3/2}F'=5$ to the ground state is always to the ground-state hfs level $6S_{1/2}F=4$, not to the other ground-state hfs level $6S_{1/2}F=3$. Therefore, the magnetic sublevels of the hfs levels $6S_{1/2}F=4$ and $6P_{3/2}F'=5$ form a closed set, which is used for laser cooling in magneto-optical traps [12].

We introduce the notation $e=e_{M'}=F'M'$ and $g=g_M=FM$ for the magnetic sublevels of the hfs levels F' and F,

respectively. The interaction of the multilevel atom with the classical coherent field is characterized by the Rabi frequencies $\Omega_{eg}^{(I)}=(\mathbf{d}_{eg}\cdot\boldsymbol{\mathcal{E}})/\hbar=\Sigma_{l=0,\pm1}(-1)^l d_{eg}^{(l)}\mathcal{E}_{-l}/\hbar$. Here, $d_{eg}^{(l)}$ with $l=0,\pm1$ is the l spherical tensor component of the dipole moment for the transition between the magnetic sublevels e and g [13,14]. Note that $d_{eg}^{(l)}$ is nonzero only if $l=M_e-M_g=0,\pm1$. Therefore, $\Omega_{eg}^{(I)}$ is nonzero only if $M_e-M_g=0,\pm1$. Hence, we have $\Omega_{eg}^{(I)}=(-1)^l d_{eg}^{(l)}\mathcal{E}_{-l}/\hbar$, where $l=M_e-M_g=0,\pm1$. In terms of the Rabi frequencies $\Omega_{eg}^{(I)}$, the Hamiltonian for the atom–field interaction can be written as

$$H_{\text{int}}=-\frac{\hbar}{2}\sum_{eg}(\Omega_{eg}^{(I)}\sigma_{eg}^{(I)}+\text{H.c.}), \tag{2}$$

where $\sigma_{eg}^{(I)}=|e\rangle\langle g|$. This Hamiltonian will be used to derive the basic equations for the atom in Sec. III.

III. EQUATIONS OF MOTION FOR THE ATOM

The interaction between the atom and the evanescent field affects not only the internal state but also the position and velocity of the atom. In this section, we present the basic equations of motion for the internal state and center of mass of the atom.

A. Equations for the internal-state density matrix

We first consider the internal state of the atom. We call $\rho^{(I)}$ the density operator of the atomic internal state in the interaction picture. The evolution of the matrix elements of $\rho^{(I)}$ is governed by the generalized Bloch equations given in Ref. [8]. When we use the transformation

$$\rho_{ee'}=\rho_{ee'}^{(I)}e^{i(M_e-M_{e'})\varphi},$$

$$\rho_{gg'}=\rho_{gg'}^{(I)}e^{i(M_g-M_{g'})\varphi},$$

$$\rho_{ge}=\rho_{ge}^{(I)}e^{i\beta z}e^{i(M_g-M_e+1)\varphi}, \tag{3}$$

we find from the Hamiltonian (2) the equations

$$\dot{\rho}_{e_ke_l}=\frac{i}{2}\sum_j(\Omega_{e_kg_j}\rho_{g_je_l}-\Omega_{g_je_l}\rho_{e_kg_j})-\frac{1}{2}\sum_j(\Gamma_{e_ke_j}\rho_{e_je_l}+\Gamma_{e_je_l}\rho_{e_ke_j})+i(M_k-M_l)\dot{\varphi}\rho_{e_ke_l}, \tag{4a}$$

$$\dot{\rho}_{g_kg_l}=-\frac{i}{2}\sum_j(\Omega_{e_jg_l}\rho_{g_ke_j}-\Omega_{g_ke_j}\rho_{e_jg_l})+\sum_{i,j}\Gamma_{e_je_ig_lg_k}\rho_{e_ie_j}+i(M_k-M_l)\dot{\varphi}\rho_{g_kg_l}, \tag{4b}$$

$$\dot{\rho}_{g_ke_l}=-\frac{i}{2}\sum_j\Omega_{g_je_l}\rho_{g_kg_j}+\frac{i}{2}\sum_j\Omega_{g_ke_j}\rho_{e_je_l}-\frac{1}{2}\sum_j\Gamma_{e_je_l}\rho_{g_ke_j}-i[\delta-\beta\dot{z}-(M_k-M_l+1)\dot{\varphi}]\rho_{g_ke_l}. \tag{4c}$$

Here, M_j is a short notation for the magnetic quantum numbers M_{e_j} and M_{g_j}, $\delta=\omega-\omega_0$ is the detuning of the field frequency ω from the atomic transition frequency $\omega_0=\omega_e-\omega_g$, and $\Gamma_{ee'gg'}$ and $\Gamma_{ee'}$ are the characteristics of spontaneous emission. The coefficients $\Gamma_{ee'gg'}$ and $\Gamma_{ee'}$ depend on r but not on z and φ. They are defined as $\Gamma_{ee'gg'}=\gamma_{ee'gg'}e^{i(M_e-M_{e'})\varphi}e^{-i(M_g-M_{g'})\varphi}$ and $\Gamma_{ee'}=\gamma_{ee'}e^{i(M_e-M_{e'})\varphi}$, where the decay parameters $\gamma_{ee'gg'}$ and $\gamma_{ee'}$ are given in Ref. [14]. In deriving Eqs. (4), we have introduced the phase-shifted field amplitudes $E_l=\mathcal{E}_l e^{-i\beta z}e^{-i(l+1)\varphi}$ and the phase-shifted Rabi frequencies $\Omega_{eg}=\Omega_{eg}^{(I)}e^{-i\beta z}e^{-i(M_g-M_e+1)\varphi}=\Sigma_{l=0,\pm1}(-1)^l d_{eg}^{(l)}E_{-l}/\hbar$. The explicit expressions for E_l are $E_{-1}=\sqrt{2}i\mathcal{N}(1-s)K_0(qr)$, $E_0=\mathcal{N}(2q/\beta)K_1(qr)$, and $E_1=-\sqrt{2}i\mathcal{N}(1+s)K_2(qr)$. Since the transformed field amplitudes E_l are independent of z and φ, so are the transformed Rabi frequencies Ω_{eg}.

The expression in the last line of Eq. (4c) contains the conventional axial Doppler shift

$$\delta_{\text{axial}}=\beta\dot{z} \tag{5}$$

and the *azimuthal* Doppler shift

$$\delta_{\text{azimuth}}^{g_ke_l}=(M_k-M_l+1)\dot{\varphi}. \tag{6}$$

Meanwhile, Eqs. (4a) and (4b) show that the azimuthal motion of the atom leads the relative frequency shifts

$$\delta_{\text{azimuth}}^{e_ke_l}=\delta_{\text{azimuth}}^{g_kg_l}=(M_k-M_l)\dot{\varphi} \tag{7}$$

for the upper-sublevel pair $\{e_k,e_l\}$ and the lower-sublevel pair $\{g_k,g_l\}$.

The axial Doppler shift (5) is a frequency shift that would arise from a plane wave traveling with the propagation constant β along the z axis. The azimuthal Doppler shifts (6) and (7) are directly proportional to the quantum numbers M_k-M_l+1 and M_k-M_l, respectively, which characterize the change in angular momentum of the atomic internal state. Such shifts are due to the rotational motion of the atom that generates an inertial field in a rotating frame in which the atom is at rest [15]. This inertial field acts like a fictitious magnetic field parallel to the rotation axis z. It splits the magnetic sublevels of the ground and excited states of the atom when the latter is rotating around the fiber [15].

In particular, the azimuthal Doppler shift is $\delta_{\text{azimuth}}^{g_ke_l}=0$, $\dot{\varphi}$, and $2\dot{\varphi}$ for $M_k-M_l=-1$, 0, and 1, respectively. This shift is very similar to the azimuthal Doppler shift of a two-level atom interacting with a Laguerre-Gaussian beam [16]. The difference is that the former depends on the quantum numbers of the atomic energy sublevels, whereas the latter depends on the orbital quantum number of the light beam. The reason for this difference is the following: The azimuthal Doppler shift of a transition is proportional the azimuthal-phase factor of the field component that causes the transition [16]. In the case considered here, the azimuthal-phase factor takes the different values 0, 1, and 2 for the field components $\mathcal{E}_{-1}$, $\mathcal{E}_0$, and $\mathcal{E}_1$, respectively [see Eqs. (1)]. Meanwhile, the angular momentum of each atomic energy sublevel is specified by its quantum numbers F and M. These features, combined with the angular-momentum conservation law and the transition-selection rules, lead to the factor M_k-M_l+1 in expression (6). In the case of a Laguerre-Gaussian beam [16], the azimuthal-phase factor coincides with the orbital angular number. This factor is the same for all the three spherical

tensor components of the field. Hence, the azimuthal Doppler shift of an arbitrary transition in the case of a Laguerre-Gaussian beam just depends on the orbital angular number. It does not depend on the quantum numbers of the atomic levels at all [16].

B. Equations for the center-of-mass motion

We now consider the center-of-mass motion of the atom. We perform a semiclassical treatment for this motion. In such a treatment, the center-of-mass motion is governed by the force that is calculated from the quantum internal state of the atom. The force of the light field on the atom is defined by the formula

$$\mathbf{F} = -\langle \boldsymbol{\nabla} H_{\mathrm{int}} \rangle. \tag{8}$$

Inserting Eq. (2) into Eq. (8) gives

$$\mathbf{F} = \frac{\hbar}{2} \sum_{eg} [(\boldsymbol{\nabla} \Omega_{eg}^{(I)}) \rho_{ge}^{(I)} + \mathrm{c.c.}]. \tag{9}$$

The axial component F_z of the force is a light pressure force and is given by

$$F_z = \frac{i\hbar\beta}{2} \sum_{eg} (\Omega_{eg}^{(I)} \rho_{ge}^{(I)} - \mathrm{c.c.}). \tag{10}$$

The radial component F_r of the force is a gradient force and is given by

$$F_r = \frac{\hbar}{2} \sum_{eg} \left(\frac{\partial \Omega_{eg}^{(I)}}{\partial r} \rho_{ge}^{(I)} + \mathrm{c.c.} \right). \tag{11}$$

The azimuthal component F_φ of the force is a light pressure force and is given by

$$F_\varphi = \frac{i\hbar}{2r} \left(\sum_{eg}{}' \Omega_{eg}^{(I)} \rho_{ge}^{(I)} + 2 \sum_{eg}{}'' \Omega_{eg}^{(I)} \rho_{ge}^{(I)} - \mathrm{c.c.} \right). \tag{12}$$

Here the notation Σ'_{eg} and Σ''_{eg} mean the summations under the conditions $M_e - M_g = 0$ and $M_e - M_g = -1$, respectively.

According to Eq. (10), all the three types of transitions, with $M_e - M_g = -1$, 0, or 1, can contribute to the axial pressure force F_z. This force is related to the recoil of photons with the axial wave vector $\beta\hat{\mathbf{z}}$. Indeed, in a particular case where the atom is at rest and the internal state $\rho^{(I)}$ of the atom is stationary, we have $i\Sigma_g(\Omega_{eg}^{(I)} \rho_{ge}^{(I)} - \mathrm{c.c.}) = \Sigma_{e'}(\gamma_{ee'} \rho_{e'e}^{(I)} + \mathrm{c.c.})$. Then, Eq. (10) yields $F_z = \hbar\beta\Gamma_{\mathrm{sc}}$, where $\Gamma_{\mathrm{sc}} = \Sigma_{ee'} \gamma_{ee'} \rho_{e'e}^{(I)}$ is the scattering rate of the atom.

According to Eq. (12), the transitions with $M_e - M_g = 0$ and $M_e - M_g = -1$ contribute to the azimuthal pressure force F_φ with the weight factors 1 and 2, respectively. Meanwhile, the transitions with $M_e - M_g = 1$ do not contribute to F_φ at all. The weight factors 0, 1, and 2 originate from the azimuthal-phase factors of the field spherical tensor components $\mathcal{E}_{-1}$, $\mathcal{E}_0$, and $\mathcal{E}_1$, which enable the transitions with $M_e - M_g = 1$, 0, and -1, respectively [see Eqs. (1)].

Unlike the forces F_z and F_φ, the force F_r is determined by the gradient of the field. It is related to the dynamical Stark shift of atomic energy levels. In a particular case where the field detuning δ is large compared to the Rabi frequencies and the effect of the fiber on the decay rates is negligible, we get $F_r = -\partial U_{\mathrm{opt}} / \partial r$, where $U_{\mathrm{opt}} = \hbar\delta\Sigma_{eg} |\Omega_{eg}|^2 / [4(2F+1)(\delta^2 + \gamma_0^2/4)]$ is the optical potential with γ_0 being the natural linewidth. It is clear that U_{opt} is attractive or repulsive when the detuning δ is negative or positive, respectively.

For convenience, we rewrite expressions (10)–(12) for the components of the force of light using the density matrix elements (3). The results are

$$F_z = \frac{i\hbar\beta}{2} \sum_{eg} (\Omega_{eg} \rho_{ge} - \mathrm{c.c.}),$$

$$F_r = \frac{\hbar}{2} \sum_{eg} \left(\frac{\partial \Omega_{eg}}{\partial r} \rho_{ge} + \mathrm{c.c.} \right),$$

$$F_\varphi = \frac{i\hbar}{2r} \sum_{eg} [(M_g - M_e + 1) \Omega_{eg} \rho_{ge} - \mathrm{c.c.}]. \tag{13}$$

In addition to the force of light, the van der Waals force from the fiber also acts on the atom when the latter is in a close vicinity of the fiber surface. This material-induced force is aligned along the radial direction and is given as $F_{\mathrm{vdW}} = -\partial U_{\mathrm{vdW}} / \partial r$, where U_{vdW} is the van der Waals potential of the atom outside the fiber. Note that U_{vdW} depends on the internal state of the atom. When we neglect the interference between the atomic bare states, we have $U_{\mathrm{vdW}} = U_{\mathrm{vdW}}^{(g)} \Sigma_g \rho_{gg} + U_{\mathrm{vdW}}^{(e)} \Sigma_e \rho_{ee}$, where $U_{\mathrm{vdW}}^{(g)}$ and $U_{\mathrm{vdW}}^{(e)}$ are the van der Waals potentials for ground- and excited-state atoms, respectively. According to Ref. [18], in the case of a cesium atom near a flat surface, the van der Waals coefficient $C_3^{(e)}$ for the excited state $6P_{3/2}$ is larger than the coefficient $C_3^{(g)}$ for the ground state $6S_{1/2}$ by a factor $\alpha = C_3^{(e)} / C_3^{(g)} = 1.98$. We can generalize this result to the case of a cylindrical surface by assuming that $U_{\mathrm{vdW}}^{(e)}$ and $U_{\mathrm{vdW}}^{(g)}$ have the same shape. Then we have $U_{\mathrm{vdW}}^{(e)} = \alpha U_{\mathrm{vdW}}^{(g)}$, where $\alpha = 1.98$. The van der Waals potential $U_{\mathrm{vdW}}^{(g)}$ for a ground-state cesium atom outside a fiber has been calculated [5,6,17]. Using the result for $U_{\mathrm{vdW}}^{(g)}$, we can easily calculate U_{vdW}. Note that the van der Waals interaction can influence not only the center-of-mass motion but also the transition frequency of the atom. Therefore, when the atom is in a close vicinity of the fiber surface, a surface-induced frequency shift $\delta_{\mathrm{vdW}} = U_{\mathrm{vdW}}^{(e)} - U_{\mathrm{vdW}}^{(g)} = (\alpha - 1) U_{\mathrm{vdW}}^{(g)}$ must be added to the atomic transition frequency ω_0.

Driven by the force from the guided light and the van der Waals force from the fiber, the classical motion of the center of mass of the atom is described by the equations

$$m\ddot{z} = F_z, \tag{14a}$$

$$m\ddot{r} = mr\dot{\varphi}^2 + F_r + F_{\mathrm{vdW}}, \tag{14b}$$

$$mr\ddot{\varphi} = -2m\dot{r}\dot{\varphi} + F_\varphi. \tag{14c}$$

Here m is the mass of the atom.

Equation (14a) indicates that, due to the pressure force F_z, the axial motion of the atom will be either accelerated or decelerated. Equation (14b) shows that the radial motion of

the atom is determined by the combined action of the gradient force F_r, the van der Waals force F_{vdW}, and the centrifugal force $F_{\mathrm{cf}}=mr\dot{\varphi}^2=L_z^2/mr^3$. Here $L_z=mr^2\dot{\varphi}$ is the z component of the orbital angular momentum of the atom with respect to the fiber axis. In terms of L_z, Eq. (14c) can be rewritten as $\dot{L}_z=T_z$, where $T_z=rF_\varphi$ is the torque. This torque is produced by the azimuthal component F_φ of the force of light on the atom. It makes L_z vary in time. Manipulating the torque T_z, we can produce and control the rotational motion of the center of mass of the atom around the fiber. In particular, when we want keep the rotation somewhat stable, we need to minimize T_z.

IV. NUMERICAL RESULTS

In this section, we perform numerical calculations for the internal state and center-of-mass motion of the cesium atom driven by the evanescent wave of a near-resonant light field in a counterclockwise rotating fundamental guided mode of the nanofiber. The wavelength λ of the guided light is tuned to the cesium D_2 line wavelength $\lambda_0=852$ nm. The refractive indices of the fiber and the vacuum clad are $n_1=1.45$ and $n_2=1$, respectively. For calculations, we choose the fiber radius $a=100$ nm, which is small enough that the field can penetrate to a distance of several times of a outside the fiber (see Fig. 2). The chosen values of λ and a satisfy very well the condition $a/\lambda<0.283$, which is required for trapping of atoms by the single-color technique [5].

In order to get insight into the specifics of the guided light field outside the fiber, we first illustrate in Fig. 2 the spatial variations of the axial component S_z (solid line) and the azimuthal component S_φ (dashed line) of the Poynting vector. The figure shows that S_φ is smaller than but comparable to S_z in the close vicinity of the fiber surface. In addition, we observe that S_φ decreases in space faster than S_z does. In other words, S_z penetrates into outside the fiber deeper than S_φ does. We note from the figure that, although the propagation power is as small as 10 nW, the magnitudes of the Poynting vector components S_z and S_φ in the close vicinity of the fiber surface are much larger than the saturation intensity $I_s=2\pi^2\hbar c\gamma_0/3\lambda_0^3=1.1$ mW/cm^2 for the cesium D_2 line [12]. Thus, a very small power can still produce a substantial intensity in the close vicinity of the fiber surface. This is because the light field is confined in the fundamental mode of the fiber.

We now calculate the force $\mathbf{F}$ of the guided light on the cesium atom in the case where the atom is in its steady internal state. We take into account the effect of the fiber on the spontaneous decay characteristics of the atom [14]. However, for simplicity, we temporarily neglect the effect of the van der Waals interaction on the atomic transition frequency.

We begin with the case where the atom is at rest. We derive the force by calculating the steady-state solution for Eqs. (4) and inserting the result into Eqs. (13).

We illustrate in Fig. 3 the spatial dependences of the axial, azimuthal, and radial components of the force of light on the atom. The detuning of the field from the D_2 line of the atom is $\delta/2\pi=-50$ MHz. Figures 3(a) and 3(b) show that F_φ is smaller than but comparable to F_z in the close vicinity of the fiber surface and that F_φ decreases in space faster than F_z does. Such behavior is reminiscent of the behavior of S_z and S_φ. Figure 3(c) shows that the radial component F_r, produced by a negative detuning, is an attractive force.

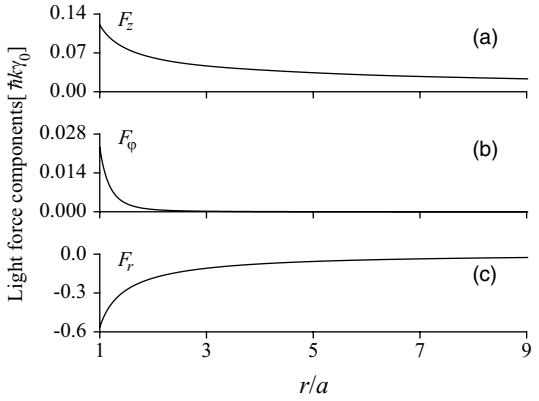

FIG. 3. Spatial dependences of the axial (a), azimuthal (b), and radial (c) components of the force of light on a cesium atom being at rest in its steady internal state outside a nanofiber. The detuning of the field from the D_2 line of the atom is $\delta/2\pi=-50$ MHz. Other parameters are as in Fig. 2.

We illustrate in Fig. 4 the frequency dependences of the axial, azimuthal, and radial components of the force of light on the cesium atom. The position of the atom is $r/a=4$. Figures 4(a) and 4(b) show that F_φ and F_z are symmetric functions of δ, with peaks at $\delta=0$. Figure 4(c) shows that F_r is an antisymmetric function of δ and is attractive, zero, or repulsive for negative, zero, or positive detuning δ, respectively.

Because of the Doppler effect and the radial variations of the field, the force $\mathbf{F}$ of the guided light depends on the velocity $\mathbf{v}=(v_r,v_\varphi,v_z)$ of the atom. We study the velocity dependence of the force. For simplicity, we limit ourselves to the case where the atom is in its local steady internal state. It is easy to calculate the dependences of $\mathbf{F}$ on v_z and v_φ since these velocity components appear explicitly in Eqs. (4). However, the dependence of $\mathbf{F}$ on v_r is hidden by the radial dependences of the Rabi frequencies and decay characteris-

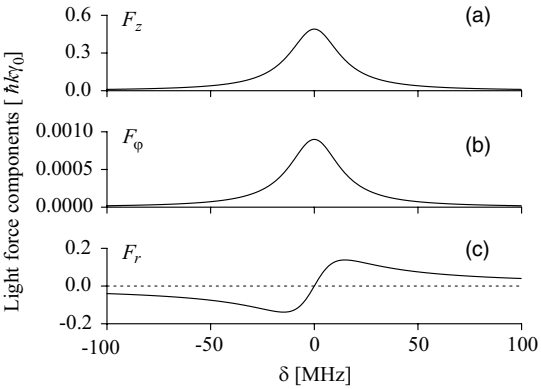

FIG. 4. Frequency dependences of the axial (a), azimuthal (b), and radial (c) components of the force of light on a cesium atom being at rest in its steady internal state outside a nanofiber. The position of the atom is $r/a=4$. Other parameters are as in Fig. 2.

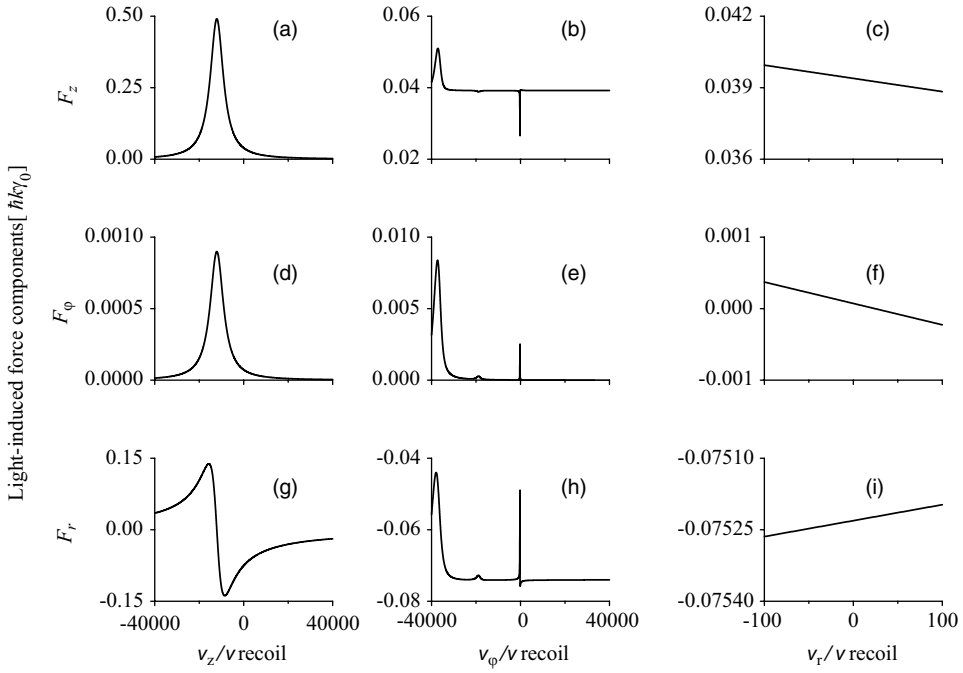

FIG. 5. Velocity dependences of the components of the force of light on a cesium atom outside a nanofiber. In the left column [(a), (d), (g)], v_z is varied, but v_φ and v_r are set to zero. In the central column [(b), (e), (h)], v_φ is varied, but v_z and v_r are set to zero. In the right column [(c), (f), (i)], v_r is varied, but v_z and v_φ are set to zero. The velocities are given in units of the recoil velocity $v_{\mathrm{recoil}}=\hbar k/m=3.52$ mm/s. The detuning of the field from the D_2 line of the atom is $\delta/2\pi=-50$ MHz. The position of the atom is $r/a=4$. The internal state of the atom is the local steady state. Other parameters are as in Fig. 2.

tics. To calculate the effect of a small velocity v_r on the force, we perform a simple linearization procedure [12]. In this procedure, we insert the formula $\dot{\rho}=\partial\rho/\partial t+v_r\partial\rho/\partial r$ into Eqs. (4), drop the time partial derivative $\partial\rho/\partial t$ in the steady-state regime, replace the operator ρ in the spatial partial derivative $\partial\rho/\partial r$ by the steady-state solution ρ_0 for an atom at rest, and solve the resulting equations for the density matrix ρ of a moving atom [12]. We note that the linearization with respect to v_r is valid when $|v_r|\Delta t/\Delta r\ll 1$, where Δt is the characteristic evolution time of the atom and Δr is the characteristic distance for the variations of the field in the radial direction. It is reasonable to take $\Delta t=\gamma_0^{-1}$ and $\Delta r=q^{-1}$. Then, the condition for the validity of the linearization procedure is $|v_r|\ll\gamma_0/q$. For a fiber with radius $a=100$ nm and a guided light field with wavelength $\lambda=852$ nm, the evanescent-wave decay parameter is $q\cong 967\ \mathrm{cm}^{-1}$. In addition, we have $\gamma_0/2\pi=5.25$ MHz. Hence, the upper limit of v_r for the linearization procedure is $\gamma_0/q\cong 341$ m/s. Such a limiting value is rather large compared to the corresponding limiting value $\gamma_0/k\cong 4.5$ m/s for the linearization in the case of an atom moving in the direction of a plane-wave light field [12]. This is because the evanescent-wave decay parameter q is small compared to the light-field wave number $k\cong 74\,000\ \mathrm{cm}^{-1}$.

We find that the velocity dependence of the force of the guided light on the atom is very complicated. It has different specifics in different ranges of detuning, atomic position, and propagation power. As an example, we plot in Fig. 5 the components of $\mathbf{F}$ as functions of v_z (left column), $v_\varphi=r\dot{\varphi}$ (central column), and v_r (right column) for the parameters $\delta/2\pi=-50$ MHz, $r/a=4$, and $P_z=10$ nW.

The left column of Fig. 5 [parts (a), (d), and (g)] shows that, when plotted as functions of the axial velocity v_z, the force components F_z and F_φ have a resonant structure and the component F_r has a dispersive behavior. Such features are observed in the vicinity of the point $v_z=-12\,100v_{\mathrm{recoil}}$, where the axial Doppler shift compensates the field detuning, that is, where $\beta v_z=\delta$. The resonant behavior of F_z and F_φ is typical for pressure forces, while the dispersive behavior of F_r is typical for gradient forces [12].

Figures 5(b), 5(e), and 5(h) show that the dependence of the force $\mathbf{F}$ on the azimuthal velocity v_φ possesses several resonances. The reason is that, unlike the axial Doppler effect, the azimuthal Doppler effect produces various frequency shifts in Eqs. (4a)–(4c). The strongest resonance, observed in the vicinity of $v_\varphi=-38\,000v_{\mathrm{recoil}}$, is due to the compensation of the field detuning δ by the azimuthal Doppler shift $\delta^{g_k e_l}_{\mathrm{azimuth}}=\dot{\varphi}=v_\varphi/r$ for the transitions with $M_l=M_k$. The weakest resonance, observed in the vicinity of $v_\varphi=-19\,000v_{\mathrm{recoil}}$, is due to the compensation of the field detuning δ by the azimuthal Doppler shift $\delta^{g_k e_l}_{\mathrm{azimuth}}=2\dot{\varphi}=2v_\varphi/r$ for the transitions with $M_l=M_k-1$. The sharp resonance observed in the vicinity of $v_\varphi=-240v_{\mathrm{recoil}}$ is related to effect of the azimuthal Doppler shift on two-photon processes. Since the effective two-photon Rabi frequency is of the form $\Omega_{ge}\Omega_{eg'}/\delta$, the position of the sharp resonance in Figs. 5(b), 5(e), and 5(h) is directly proportional to the field intensity and inversely proportional to the field detuning. Thus, the influence of v_φ on the force of the guided light is more complicated than the influence of v_z.

The linearity of the curves for the components of the force $\mathbf{F}$ in Figs. 5(c), 5(f), and 5(i) is a result of the linearization procedure with respect to the radial velocity v_r [12]. Such a procedure allows us to calculate $\mathbf{F}$ only up to first order in v_r.

When the field detuning is large enough, the motion of the atom along the radial direction r can be described by an effective potential $U_{\mathrm{rad}}=U_{\mathrm{opt}}+U_{\mathrm{cf}}+U_{\mathrm{vdW}}$, which is comprised of the optical potential U_{opt}, the centrifugal potential $U_{\mathrm{cf}}=L_z^2/2mr^2$, and the van der Waals potential U_{vdW} [5,6,17]. We plot in Fig. 6 the potential U_{rad} for the parameters

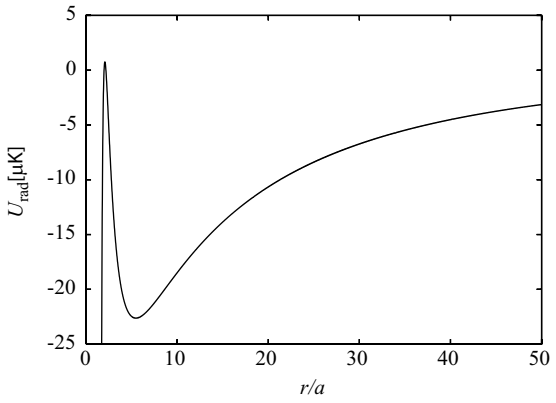

FIG. 6. Total effective potential U_{rad} for the radial motion of a cesium atom. The detuning of the field from the D_2 line of the atom is $\delta/2\pi=-50$ MHz. The orbital angular momentum of the atom is $L_z=43\hbar$. Other parameters are as in Fig. 2.

$\delta/2\pi=-50$ MHz and $L_z=43\hbar$. As seen from Fig. 6, U_{rad} has a deep minimum point at the distance $r_m=5.47a=547$ nm from the fiber axis, not only well outside the fiber but also outside the range of substantial action of the van der Waals force. We note that, in the region of $r\cong a$, the shape of U_{rad} is similar to that of the van der Waals potential U_{vdW}. However, in the region of $r>3a$, U_{vdW} is weak and, therefore, U_{rad} practically coincides with the sum of U_{opt} and U_{cf}. The minimum of U_{rad} is formed at a point where the centrifugal force F_{cf} compensates the gradient force F_r.

When the detuning of the field is not too large and the distance from the atom to the fiber is not too far, the atom undergoes not only the gradient force but also the axial and azimuthal pressure forces of light. The axial force F_z and the azimuthal force F_φ can accelerate or decelerate the axial and azimuthal motions, respectively. They can also affect the internal state through the axial and azimuthal Doppler shifts, respectively. The torque T_z, produced by the azimuthal force F_φ, leads to an increase or decrease of the angular momentum of the atom. When we control the torque T_z appropriately, we can manipulate the rotational motion of the atom.

When T_z is large, the angular momentum of the atom and, consequently, the centrifugal force increase quickly. The resulting imbalance between the centrifugal and gradient forces will quickly accelerate the atom in the radial direction. Then, the atom will quickly go away from the fiber. Therefore, in order to produce a long-lived rotational motion of the atom around the fiber, we need to balance the centrifugal force by a gradient force from one hand and to minimize the torque from the other hand.

We plot in Fig. 7 the trajectory of a rotational motion of the atom around the fiber. The parameters for the fiber and the light field are as in Fig. 6. The atom is initially positioned at a point near to the minimum point of the potential U_{rad} in Fig. 6. The initial velocity of the atom is in the range of thermal velocities at 5 μK. The transverse component of the initial velocity corresponds to the angular momentum $L_z=43\hbar$, which is necessary for producing the centrifugal component of the trapping potential in Fig. 6. In these calculations, we include the time evolution of the internal state of the atom, which is initially prepared in the ground-state hfs level $6S_{1/2}F=4$, with a flat (incoherent) distribution with respect to the magnetic sublevels. We also take into account the effects of the van der Waals interaction on the center-of-mass motion and transition frequency of the atom. To get a good resolution for the three-dimensional trajectory and trajectory mapping, the evolution time is limited to 300 μs. The figure shows that the atom is kept around the fiber in a rotational motion.

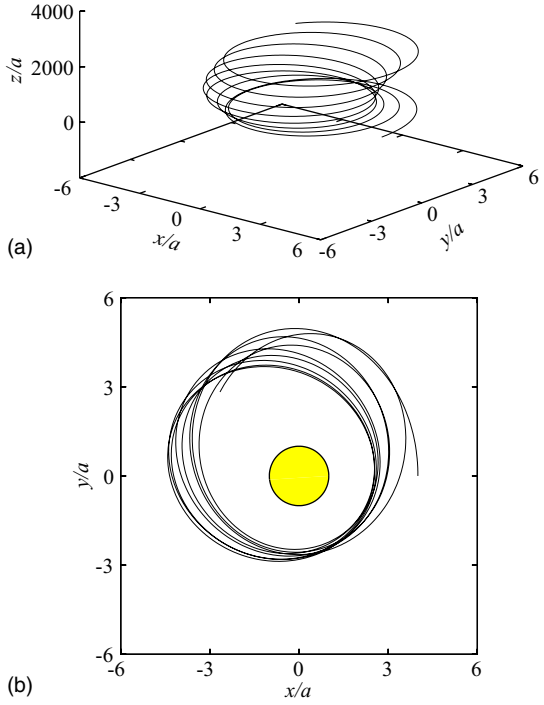

FIG. 7. (Color online) Three-dimensional trajectory (a) and trajectory mapping (b) of a cesium atom spinning around a nanofiber (shadowed area). The initial position and the initial velocity of the atom are $(x=4a, y=0, z=0)$ and $(v_x=0, v_y=14.6v_{rec}, v_z=20v_{rec})$, respectively. The detuning is $\delta/2\pi=-50$ MHz. The evolution time is 300 μs. Other parameters are as in Fig. 2.

Figure 8 extends the duration of the atomic center-of-mass motion of Fig. 7 for a longer time, namely, 2 ms. As seen, the atom can rotate many times around the fiber. The time during which the atom is kept in the rotational motion around the fiber is a macroscopic time (>2 ms). The orbit of each loop is quasi-elliptical. With increasing time, the orientation of the loop rotates slowly and the size of the orbit becomes broader. The increase of the size of the orbit is mainly due to the increase of the orbital angular momentum of the atom.

We plot in Fig. 9 the axial angular momentum L_z of the atom as a function of time. Figure 9 shows that the angular momentum of the atom increases slowly with time. Such increase of L_z is due to the action of the azimuthal force F_φ or, equivalently, the torque T_z. To prolong the bounding of the atom to the fiber, we need to minimize T_z. When T_z is large, L_z increases quickly and, consequently, the atom quickly goes away from the fiber.

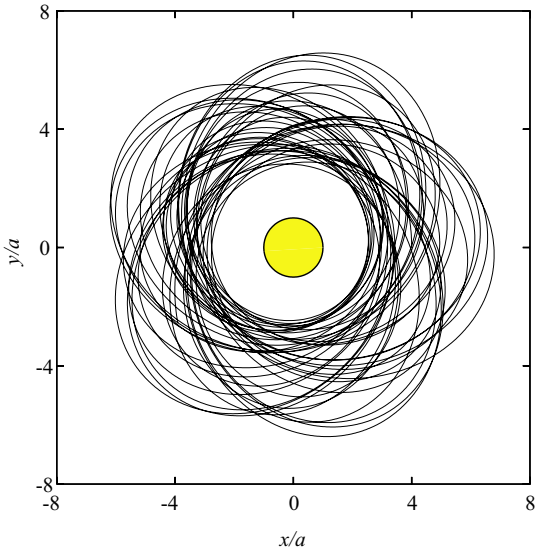

FIG. 8. (Color online) Trajectory mapping of a cesium atom spinning around a nanofiber. The evolution time is 2 ms. Other parameters are as in Fig. 7.

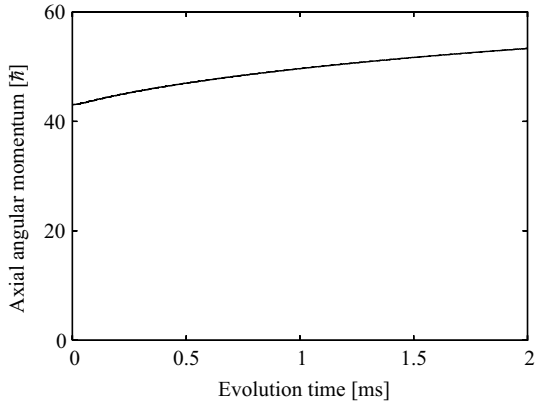

FIG. 9. Axial angular momentum L_z of a spinning cesium atom as a function of time. Other parameters are as in Fig. 7.

V. SUMMARY

In conclusion, we have studied the action of the light-induced force and torque on a cesium atom outside a nanofiber. We have derived a set of coupled equations for the internal state and center-of-mass motion of the atom. In addition to the axial Doppler effect, the azimuthal Doppler effect has been revealed. We have calculated the pressure and gradient forces as functions of various parameters, such as the distance between the atom and the fiber, the detuning of the field, and the velocity of the atom. We have demonstrated that the evanescent light field in a circular fundamental guided mode can force the atom to rotate around the nanofiber for a macroscopic time. The enhancement of the spontaneous decay rates and the effect of the van der Waals potential have been taken into account in our calculations. We have found that, due to the action of the torque, the angular momentum of the atom increases with increasing time. Our work shows that nanofibers can be used to produce, manipulate, and control the rotational motion of atoms.

ACKNOWLEDGMENTS

This work was carried out under the 21st Century COE program on "Coherent Optical Science." V.I.B. was also partly supported by INTAS project (Grant No. 479).

[1] R. Folman, P. Kruger, J. Schmiedmayer, J. Denschlag, and C. Henkel, Adv. At., Mol., Opt. Phys. **48**, 263 (2002).
[2] S. Eriksson, M. Trupke, H. F. Powell, D. Sahagun, C. D. J. Sinclair, E. A. Curtis, B. E. Sauer, E. A. Hinds, Z. Moktadir, C. O. Gollasch, and M. Kraft, Eur. Phys. J. D **35**, 135 (2005).
[3] C. Henkel and M. Wilkens, Europhys. Lett. **47**, 414 (1999).
[4] M. P. A. Jones, C. J. Vale, D. Sahagun, B. V. Hall, and E. A. Hinds, Phys. Rev. Lett. **91**, 080401 (2003); P. K. Rekdal, S. Scheel, P. L. Knight, and E. A. Hinds, Phys. Rev. A **70**, 013811 (2004).
[5] V. I. Balykin, K. Hakuta, Fam Le Kien, J. Q. Liang, and M. Morinaga, Phys. Rev. A **70**, 011401(R) (2004).
[6] Fam Le Kien, V. I. Balykin, and K. Hakuta, Phys. Rev. A **70**, 063403 (2004).
[7] See, for example, D. Marcuse, *Light Transmission Optics* (Krieger, Malabar, FL, 1989).
[8] Fam Le Kien, V. I. Balykin, and K. Hakuta, Phys. Rev. A **73**, 013819 (2006).
[9] Fam Le Kien, J. Q. Liang, K. Hakuta, and V. I. Balykin, Opt. Commun. **242**, 445 (2004).
[10] Fam Le Kien, V. I. Balykin, and K. Hakuta, Phys. Rev. A **73**, 053823 (2006).
[11] See, for example, J. D. Jackson, *Classical Electrodynamics*, 3rd ed. (Wiley, New York, 1999).
[12] H. J. Metcalf and P. van der Straten, *Laser Cooling and Trapping* (Springer, New York, 1999).
[13] See, for example, B. W. Shore, *The Theory of Coherent Atomic Excitation* (Wiley, New York, 1990).
[14] Fam Le Kien, S. Dutta Gupta, V. I. Balykin, and K. Hakuta, Phys. Rev. A **72**, 032509 (2005).
[15] J. Dalibard and C. Cohen-Tannoudji, J. Opt. Soc. Am. B **6**, 2023 (1989).
[16] L. Allen, M. J. Padgett, and M. Babiker, Prog. Opt. **39**, 291 (1999); A. R. Carter, M. Babiker, M. Al-Amri, and D. L. Andrews, Phys. Rev. A **73**, 021401(R) (2006).
[17] M. Boustimi, J. Baudon, P. Candori, and J. Robert, Phys. Rev. B **65**, 155402 (2002); M. Boustimi, J. Baudon, and J. Robert, *ibid.* **67**, 045407 (2003).
[18] M. Chevrollier, M. Fichet, M. Oria, G. Rahmat, D. Bloch, and M. Ducloy, J. Phys. II **2**, 631 (1992); M. Fichet, F. Schuller, D. Bloch, and M. Ducloy, Phys. Rev. A **51**, 1553 (1995).